Hindawi
Geofluids
Volume 2023, Article ID 3832452, 16 pages
https://doi.org/10.1155/2023/3832452

Research Article

Pore-Throat Structure and Fractal Characteristics of Tight Sandstones: A Case Study from the Chang 6_3 Sublayer, Southeast Ordos Basin

Zhuo Han,[1] Yanan Zhou,[1,2] Fanrong Wei,[3] Qian Zhang,[1,4] Pingtian Fan,[5] Chao Deng,[1] Jiantao Gong,[3] Xin Cheng,[1] Erping Ma,[6] and Hanning Wu[1]

[1]*State Key Laboratory of Continental Dynamics, Department of Geology, Northwest University, Xi'an 710069, China*
[2]*Shandong Key Laboratory of Depositional Mineralization and Sedimentary Mineral Shandong University of Science and Technology, Qingdao, Shandong 266590, China*
[3]*Exploration Department of Yanchang Oilfield, Yan'an, Shaanxi 716000, China*
[4]*No.5 Oil Recovery Plant of PetroChina Changqing Oilfield Company, Xi'an, Shaanxi 710201, China*
[5]*Nanniwan Oil Production Plant of Yanchang Oilfield, Yan'an, Shaanxi 716007, China*
[6]*Research Institute of Shaanxi Yanchang Petroleum (Group) Co. Ltd., Xi'an, Shaanxi 710065, China*

Correspondence should be addressed to Yanan Zhou; zhouyanan@nwu.edu.cn

Received 13 June 2022; Revised 7 August 2022; Accepted 8 September 2022; Published 20 March 2023

Academic Editor: Wenhui Li

Copyright © 2023 Zhuo Han et al. This is an open access article distributed under the Creative Commons Attribution License, which permits unrestricted use, distribution, and reproduction in any medium, provided the original work is properly cited.

The micropore-throat structure is a controlling factor on the capacity of storage and seepage for the tight sandstone reservoirs. Therefore, quantitatively analyzing the pore-throat structure is crucial for realizing the oil accumulated in the tight reservoirs. To study the micropore-throat, a battery of experiments such as casting thin sections, scanning electron microscopy, high-pressure mercury injection, and the petrophysical characteristics of reservoirs were conducted on ten samples gathered in the Late Triassic Chang 6_3 sublayer in the Southeast Ordos Basin, China. The main pore types of the samples are intergranular pores, feldspar dissolved pores, and intergranular dissolved pores. Meanwhile, the pore-throat structure of each sample was identified as large pores, medium pores, and small pores by combining the result of HPMI with fractal theory. The corresponding mean values of the fractal dimension D for large, medium, and small pores are 2.83, 2.69, and 2.31, respectively, indicating that the complex structure and strong heterogeneity were presented in the large pores according to the maximum fractal dimension. In addition, the fractal dimension of the medium pores (D_{P-2}) has a negative correlation with porosity, permeability, median pore-throat radius, maximum mercury saturation, mercury withdrawal efficiency, displacement pressure, and content of quartz, while a positive correlation with feldspar content, sorting coefficient, and coefficient of variation. Thus, the reservoir space and seepage capacity of all samples in this study were determined by the size, complexity, and distribution of the medium pores. Furthermore, the content of quartz contributes to the storage of the reservoir and the homogeneity of the pore-throat structure, thereby the storage capacity improves with the increase of quartz content. Feldspar dissolution pores are developed widely in the study area, leading to various pores with diverse types, sizes, complex structures, and large fractal dimensions. Although the storage capacity of tight sandstone reservoirs was enhanced with increasing feldspar content, the pore-throat structure complexity was also stronger, resulting in the reduction seepage capacity of fluid.

1. Introduction

Given the increasing demand for fossil energy, the exploration and development of unconventional resources, for instance, tight oil and gas have drawn more attention worldwide [1, 2]. Compared to the successful development of tight oil in North America, China just started out and has a promising future in view of the current investigation and reevaluation on its reserves [3]. The tight oil is usually preserved in a tight sandstone reservoir, defined as a reservoir with

permeability and porosity of less than 1 mD and 10 percent, respectively [4]. The micropore-throat structure significantly affects the storage capacity and seepage ability of tight sandstone reservoirs. However, it is hard to characterize the micropore-throat structure owing to its poor physical properties and strong heterogeneous [5–8].

Experimental methods are conducted to evaluate the pore-throat structure, such as image observation methods represented by scanning electron microscopy (SEM) and casting thin sections (CTS), photoelectromagnetic radiation methods by nuclear magnetic resonance (NMR) and CT scanning, and fluid injection method by N_2 gas adsorption measurements and high-pressure mercury injection (HPMI) as well as constant-rate mercury injection (CRMI) [9–16]. Considering the complex pore-throat characteristics and strong heterogeneity caused by complicated deposition and diagenesis processes, it is hard to identify the micropore-throat structure of tight sandstone reservoirs by a single method [5, 17–26]. For instance, although the image observation methods (SEM and CTS) can directly observe the geometry and the size of the pore-throat within sight, its visual field is too narrow to represent the whole sample [27]. CRMI characterizes the pore-throat structure by monitoring changes in pressure and saturation, whereas, it assumed a sphere pore space to calculate its pore radius, which is different from the real pore throat distribution in the reservoirs [28]. N_2 gas adsorption mainly identifies the pore-throat structure at a nanoscale scale with a limited zone of pores radius [29]. In comparison, the acquired HPMI parameters coupled with fractal theory are of great significance in both qualitatively evaluating the pore-throat structure [29, 30] and quantitatively describing the complexity of pore-throat structure [31–33]. Together with image observation, HPMI, and fractal analysis, this study aims at building a bridge between the micropore-throat structure and macroquality of the reservoir to analyze the characteristics of pore-throat structure.

To identify the complexity of pore-throat structure, a variety of experiments, including petro-physical characteristics of reservoir, SEM, CTS, and HPMI were implemented on ten samples gathered in the Chang 6_3 sublayer, Yanchang Formation of southeast of Ordos Basin. The structure of the pore-throat was quantitatively analyzed based on new experimental results. Meanwhile, the fractal dimensions $D_{P\text{-}1}$, $D_{P\text{-}2}$, and $D_{P\text{-}3}$ were calculated to discuss the complexity and heterogeneity of the Chang 6_3 sublayer. The conclusion of this study can give some reference for the exploration of tight sandstone reservoirs.

2. Geological Setting

Located in the west of the North China Craton, the Ordos Basin (Figures 1(a) and 1(b)) is famous for its large reserves of unconventional resources [34, 35]. In this basin, the Paleozoic, Mesozoic, and Cenozoic sedimentary rocks were covered on the Archean and Proterozoic metamorphic crystalline basements [36, 37]. Multiple sets of oil and gas combinations were well preserved from the Paleozoic to Mesozoic sedimentary strata in the Ordos Basin [38]. In which the Upper Triassic Yanchang Formation is the most vital reservoir for the exploration and development of tight oil and gas. The Yanchang Formation deposited in a lacustrine-delta environment contains ten members (Chang 10 to Chang 1, towards the top) [39]. Generally, in this basin, the tight oil is mainly accumulated in the Chang 6_3 sublayer, Chang 7 layer, and Chang 8_1 sublayer.

Located in the southeast of Yishan slope, Ordos Basin, the tectonic characteristics of the study area (Figure 1(a)) are west-inclined monocline with a dip angle less than 1°. In this area, the Chang $4{+}5_2$ sublayer and Chang 6 layer are the main oil producing layers. According to the characteristics of the standard layer and sedimentary cycle, the Chang 6 layer is divided into four oil sublayers, among which the Chang 6_3 sublayer is a tight sandstone reservoir with a thickness of about 26-40 meters and the lithology is mainly terrigenous clastic rocks, including mudstone and medium-fine sandstone in the study area. The underwater distributary channel sand body would be a favorable oil and gas reservoir. [40]. The porosity of the Chang 6_3 sublayer in the study area ranged from 1.54% to 10.83%, with a mean value of 6.39% while the permeability of most samples is below 0.30 mD, with a mean value of 0.04 mD, which shows a typical feature of a tight sandstone.

3. Materials and Methods

3.1. Sampling and Processing. Ten samples were collected from the Late Triassic Chang 6_3 sublayer of Yanchang Formation in southeast of the Yishan slope, as shown in Figure 1(c). These samples were firstly drilled into cylinders of about 2.5 cm in diameter and 3.0 cm in length, respectively. Then extraction experiments were carried out in alcohol and benzene after numbering these samples. Then, drying at 50°C for 24 hours, samples were cut into two segments, one part of 2.5 cm in length for helium porosity, nitrogen permeability measurements, and HPMI test while the other part of 0.5 cm in length for CTS and SEM observations.

3.2. Experimental Measurements

3.2.1. SEM Observation. The image of SEM can directly reflect characteristics of pore-throat structure, interstitial material, pore types, and cementation types. SEM observation was carried out by MAIA-3 instrument of Tescan field emission electron microscope in the Geological Experiment Test and Analysis Center (GETAC) of Xi'an Shiyou University (XSYU).

3.2.2. CTS Observation. The pores of the cylindrical samples (0.5 cm in length) were filled with blue casting as well as dye agent and processed into casting thin sections with 0.03 mm in thickness. Based on the CTS analysis, the mineral composition, interstitial material, pore types, and cementation types can be confirmed, and the size of the pores, throats, and grains can be quantitatively characterized [27]. In this study, the CTS of ten typical samples was observed by LEICA 4P research polarizing microscope in the GETAC, XSYU, Xi'an, China.

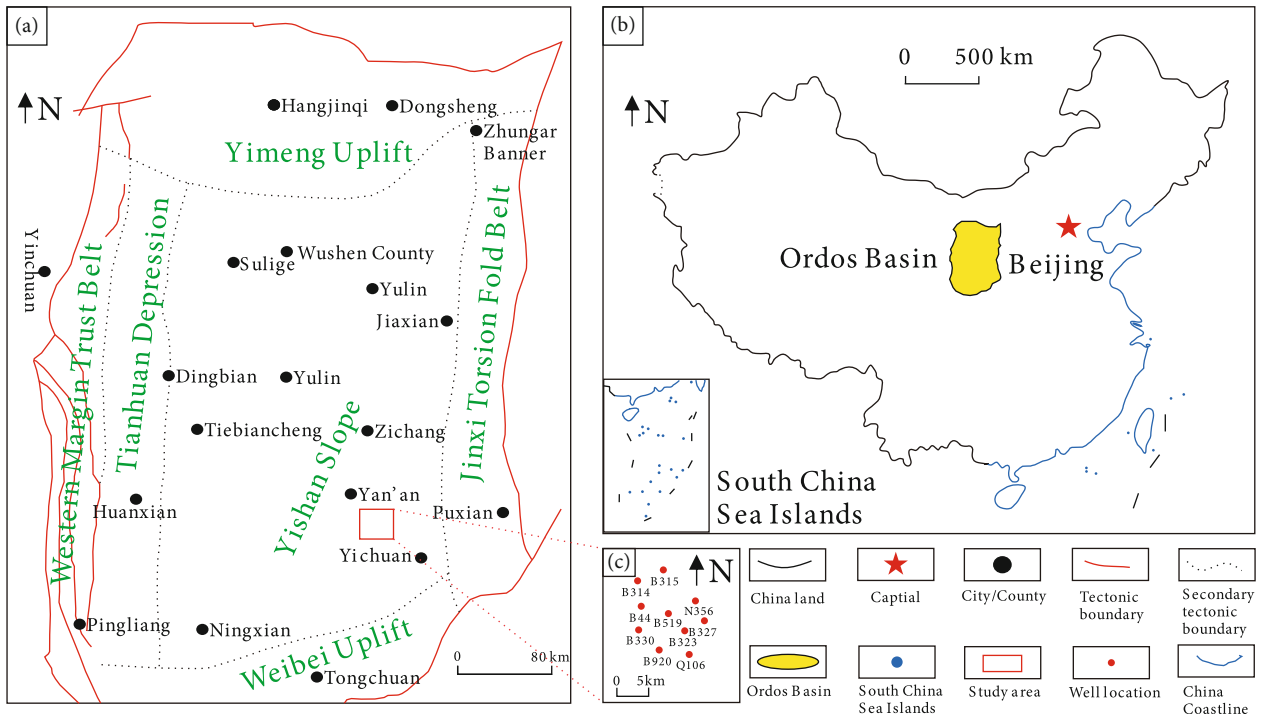

Figure 1: Location of the study area and sampling points in the Ordos Basin (modified from [19]).

3.2.3. HPMI Experiment. The distribution of pore volume fraction of different pore sizes was obtained from HPMI analysis for reservoir evaluation [29, 30]. As a nonwetting phase fluid of rocks, mercury was injected into the pores of samples, because the injection pressure overcame the capillary resistance of the pore-throat. When they are equal to each other, the injection pressure and the volume of the injected mercury are measured, which can be used to plot a capillary pressure curve. Therefore, the parameters of pore-throat structure were obtained to analyze petrophysical characteristics, complexity of pore-throat, and fractal features further [31]. The HPMI experiment was performed on five typical samples by using the American MAC AutoPore IV 9505 Automatic Mercury Injection instrument following the GB/T29171-2012 standard. The maximum mercury injection pressure reached up to 200 MPa and the measured maximum pore-throat radius was about 3.6 nm.

3.3. Fractal Theory. In the fractal theory, the most important feature is self-similarity, which is a self-similar object that has similar structural features at different scales. Self-similar objects with fractal characteristics are represented by fractal dimension D_f or D, which were greatly applied to quantitatively identify the heterogeneity and complexity of the pore-throat structure [19–23, 34–37]. Generally, the value of fractal dimension ranges between 2 to 3, increasing with the heterogeneity and complexity of pore-throat structure [41–46]. Accordingly, if the pore-throat structure has fractal characteristics, the amount of pore-throats which radiuses exceeded r can be calculated. Then, the relevant formula can be expressed as follows, and its instructions on parameters are detailed in relevant references [19–23]:

$$N(>r) = \int_r^{r_m} P(r)dr = ar^{-D}, \tag{1}$$

where $N(>r)$ is the amount of pore-throats with a radius more than r; r_m is the maximum radius of pore (μm); $P(r)$ is the distribution function of pore radius; a is scale constant; D is the fractal dimension.

Equation (2) is obtained by performing the derivation of r in Equation (1):

$$P(r) = \frac{dN(>r)}{dr} = (-D \times a)r^{-D-1}. \tag{2}$$

By transforming Equation (2) into Equation (3), the total volume $V(<r)$ of pores with a radius lower than r can be expressed:

$$V(<r) = \int_{r_s}^{r} P(r)ar^3 dr = \frac{-a^2 D}{3-D}\left(r^{3-D} - {r_s}^{3-D}\right), \tag{3}$$

where r_s is the minimum pore radius (μm).

The total pore volume (V) can be listed as follows:

$$V = \frac{-a^2 D}{3-D}\left({r_m}^{3-D} - {r_s}^{3-D}\right). \tag{4}$$

By transforming Equations (3) and (4) into Equation (5), the cumulative volume fraction $V(c)$ of a pore-throat with

Table 1: Mineral composition and content of core samples from the Chang 6_3 sublayer of Yanchang Formation.

Quartz (%)	Feldspar (%)	Lithic (%)	Kaolinite (%)	Chlorite (%)	Illite (%)	$Q_1/(F_1+R_1)$
44.8	24.3	18.2	1.2	2.6	1.1	1.05

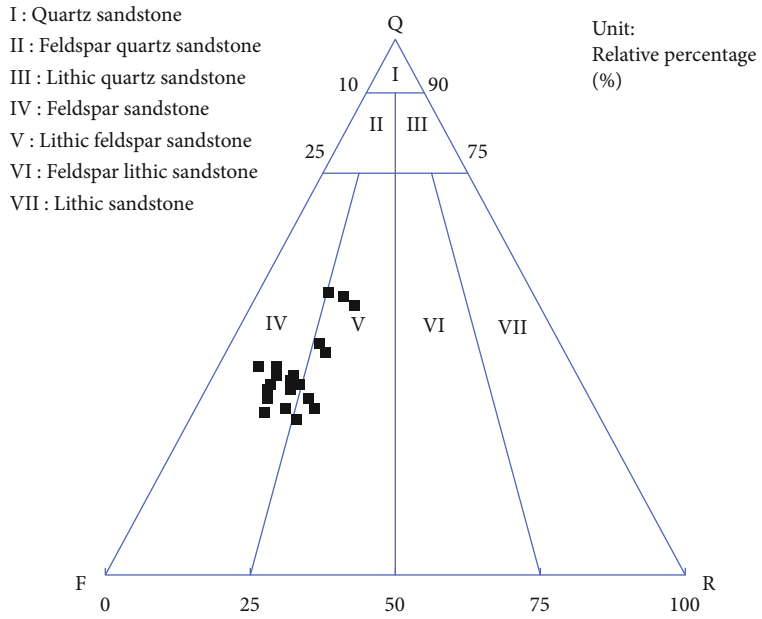

Figure 2: Triangulation of the Chang 6_3 sublayer of Yanchang Formation study area, Ordos Basin.

pore radius lower than r is obtained:

$$V(c) = \frac{V(<r)}{V} = \frac{r^{3-D} - r_s^{3-D}}{r_m^{3-D} - r_s^{3-D}}. \quad (5)$$

In the tight sandstone, r_s is much smaller than r_m, Equation (5) can be simplified as follows [29, 30]:

$$V(c) = \left(\frac{r}{r_{\max}}\right)^{3-D}. \quad (6)$$

Finally, Equation (7) can be obtained after calculating the logarithm of $V(c)$:

$$\log V(c) = \log\left(1 - S_{Hg}\right) = (3-D)\log r - (3-D)\log r_{\max}. \quad (7)$$

If the pore size distribution fits the fractal theory, there is a linear dependence between $log(1 - S_{Hg})$ and $logr$. According to the slope of the line $H = 3 - D$, D is equal to $H - 3$.

4. Results

4.1. Petrophysical Characteristics. The mineral composition and content of ten samples gathered in the study area are shown in Table 1. Combined with the sandstone classification scheme [47] and the analysis results of both SEM and CTS, the Chang 6_3 sublayer is classified as the feldspar sandstone and lithic feldspar sandstone (Figure 2). The component maturity of tight sandstone is determined by the ratio of stable component (quartz, Q_1) to unstable component (feldspar+lithic, F_1+R_1) [48], which is equal to 1.05, indicating that the component maturity of the Chang 6_3 sublayer is low.

The average content of quartz in this area (Table 1) is 44.8%, and the feldspar is 24.3%, of which plagioclase is higher, followed by potassium feldspar. In addition, the average content of lithic fragments is 18.2%, of which metamorphic, sedimentary, volcanic lithic fragments, and mica account for 44.44%, 30.95%, 2.38%, and 22.23%, respectively. Furthermore, the content of phyllite, quartzite, and slate are 1.2%, 1.9%, and 1.14%, respectively.

Clay minerals and carbonate are the main interstitial materials of the Chang 6_3 sublayer. Clay minerals mainly consist of chlorite (2.6%), followed by kaolinite (1.2%) and hydromica (1.1%), and carbonate is dominated by calcite. The characteristics of the Chang 6_3 sublayer in the study area are interpreted as follows: the particle size of debris is fine, ranging from 0.10 mm to 0.20 mm. Their sorting feature is medium, in which mainly are fine sandstone, followed by silty sandstone. And, point-point and point-line contact make up their main contact types. The cementation and support types are mainly pore cementation and particle support, respectively.

The petrophysical property analysis of Chang 6_3 sublayer in southeastern Ordos Basin shows that porosity ranged from 1.54% to 10.83% with a mean value of 6.39% (Figure 3(a)). The permeability of most samples is less than 0.30 mD with a mean value of 0.04 mD (Figure 3(b)), indicating that the Chang 6_3 sublayer is a tight sandstone in this

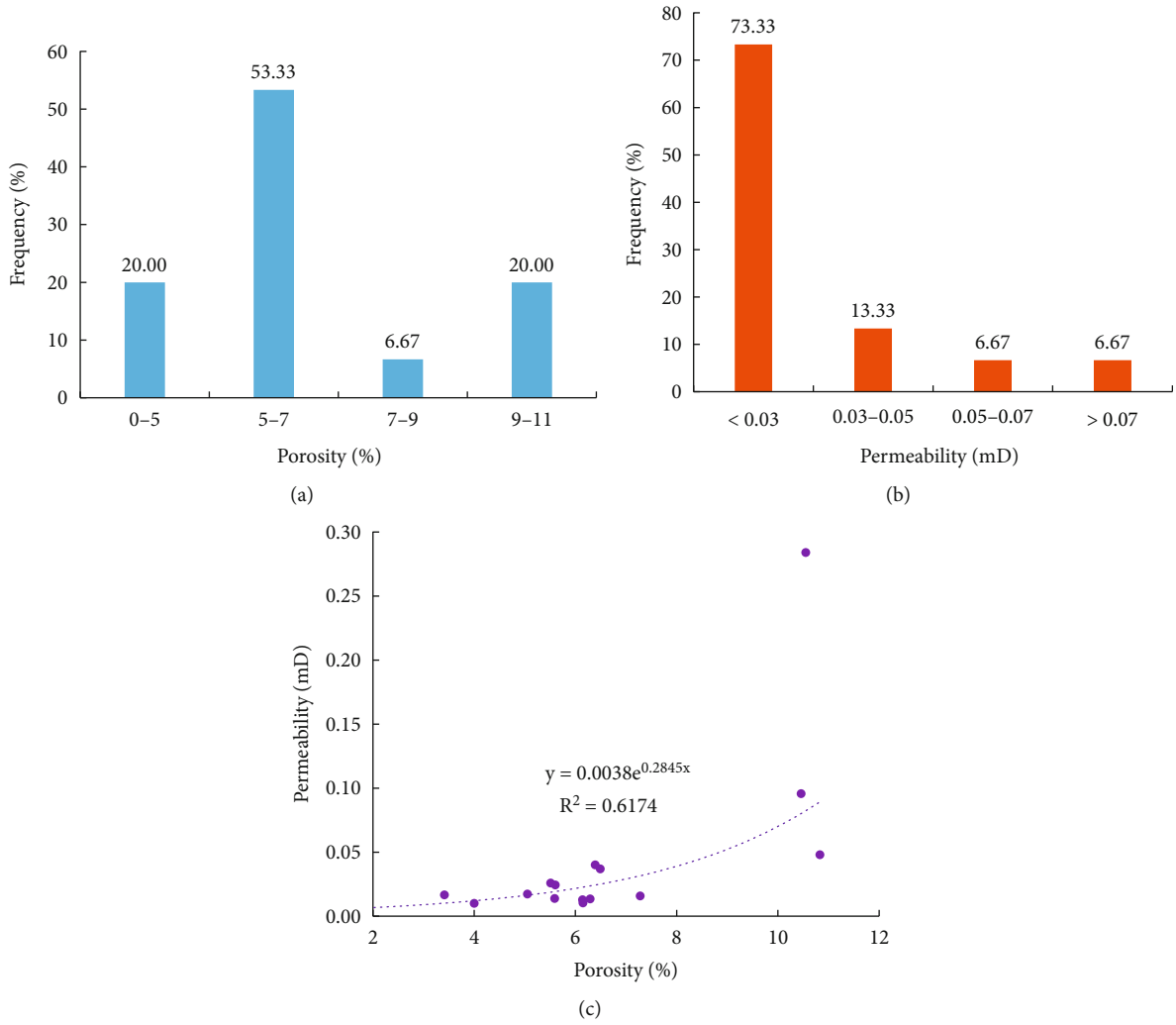

FIGURE 3: Petrophysical characteristics of Chang 6_3 sublayer of Yanchang Formation. (a) Porosity and (b) permeability distributions and (c) porosity-permeability relation.

study with low porosity and ultralow permeability. Figure 3(c) shows a weak correlation between porosity and permeability with a correlation coefficient 0.6174, hinting at that the pore-throat structure was complex and stronger heterogeneous.

4.2. Pore Characteristics. In general, the areal porosity rate is proportional to the number of pores, that is, the lower the areal porosity rate, the fewer number of pores. The CTS results of areal porosity (less than 10%) prove that the Chang 6_3 sublayer is a tight sandstone reservoir. Nevertheless, diverse types of pores were developed in the reservoir due to its strong heterogeneity, which showed irregular shapes, different sizes, and uneven distribution.

The samples in study area are characterized by micron pore-throat, and dissolution pores are more developed than residual pores based on the results of CTS and SEM. The residual pores are mainly composed of intergranular pores which show polygonal, irregular, and clear boundaries (Figure 4(a)) hinting that these pores suffered from compaction, cementation, and hybrid filling. The chlorite films (Figure 4(b)) and quartz (Figure 4(c)) are observed in our samples. It is clear that the existence of chlorite films and quartz are of great significance in resistance to compaction, thus conducive to the preservation of pores in the samples. On top of that, dissolution pores are widely developed, mainly consisting of feldspar dissolution pores and intergranular dissolved pores (Figures 4(d)–4(f)) with complex pore morphology, which improve reservoir storage space. In addition, few lithic dissolution pores as well as carbonate dissolution pores are observed, and no microcracks were found in the samples of Chang 6_3 sublayer, this means that there are strong compaction and weak tectonism.

4.3. The Results of HPMI. The capillary pressure characteristics curves and distribution curves of pore-throat radius of five representative samples were plotted based on the HPMI results (Figure 5). On the basis of the morphological characteristics of capillary pressure curves and distribution curves of pore-throat radius, the samples can be assigned to three types (Table 2).

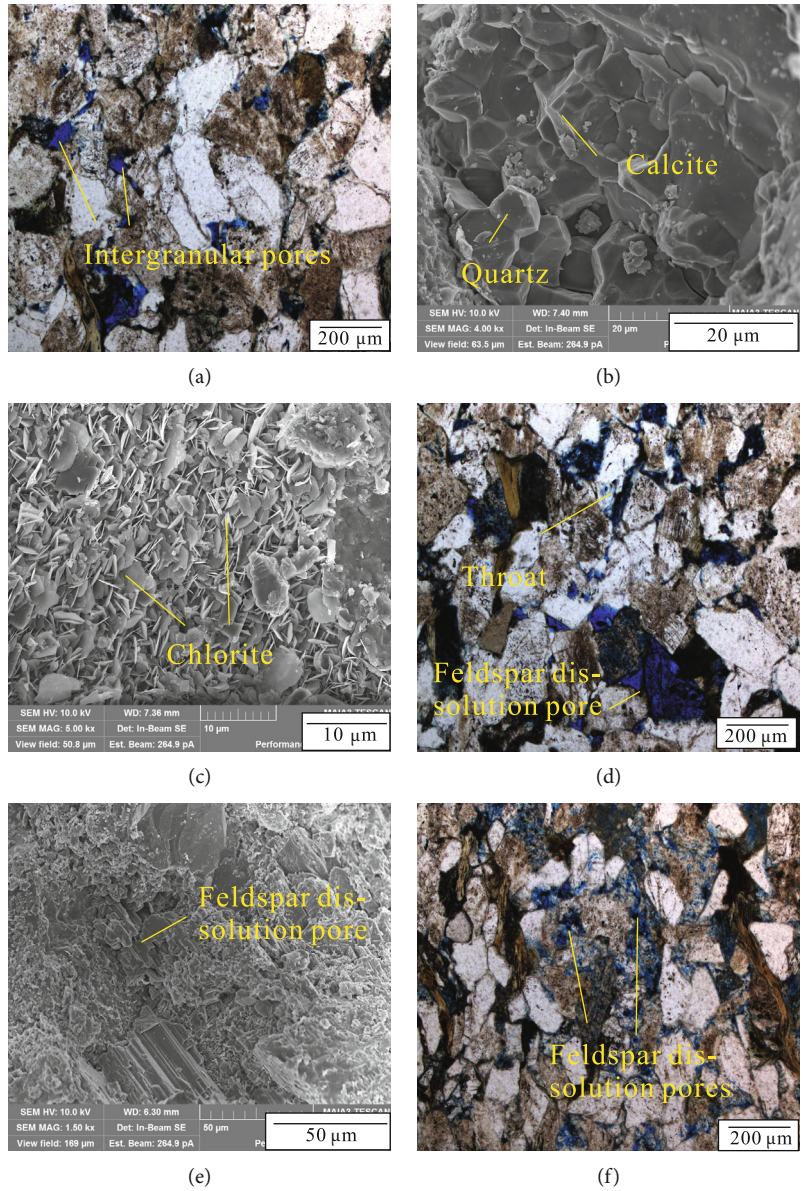

Figure 4: CTS and SEM analyses. (a) Intergranular pores, CTS. (b) Quartz cement and Calcite cement, SEM. (c) Chlorite cement, SEM. (d) Throat, CTS. (e) Feldspar dissolution pores, SEM. (f) Feldspar dissolution pores, CTS.

Type I, A1 sample shows low displacement pressure with an average of 0.4 MPa in Table 2. The capillary pressure curve of A1 reflects characteristics of the "long-flat section in the middle" (Figure 5(a)). As shown in Figure 5(b), there is a single-peak on the right side with a radius peak ranging between 0.48 μm and 0.63 μm. It shows that the sample has large size pore-throat, which makes mercury easy to be injected into the pore-throat. Type II is composed of A2 and A3 samples with an average displacement pressure of 0.56 MPa, and the relatively-short horizontal mercury injection capillary pressure curves can be observed between 1-8 MPa and 60-80 MPa (Figure 5(c)). In Figure 5(d), a double-peak is presented, in which the distribution of pore-throat radius curves on the left as well as right side are 0.015–0.04 μm and 0.1–0.48 μm, respectively, showing that these samples have pore-throat of middle size, which makes mercury not easy to be injected into the pore-throat. A4 and A5 samples are applied to type III, whose patterns (Figures 5(e) and 5(f)) are similar to the curves of type II. However, it is difficult to overcome the capillary pressure owing to the development of thin and microthroats, causing highest displacement pressure and smallest pore-throat size.

4.4. Fractal Feature. Scatter plots of log $(1 - S_{Hg})$ and log r from each sample were drawn according to the HPMI pore-throat structure parameters (Figure 6). A linear correlation between log $(1 - S_{Hg})$ and log r with correlation coefficients of more than 0.8 was observed on the basis of fractal curve [19–23]. The result illustrated that the pore-throat structure of each sample was multifractal. Based on the inflection points of the fractal curve, the curve can be split into three sections, thus dividing the pore-throat structure of samples into large,

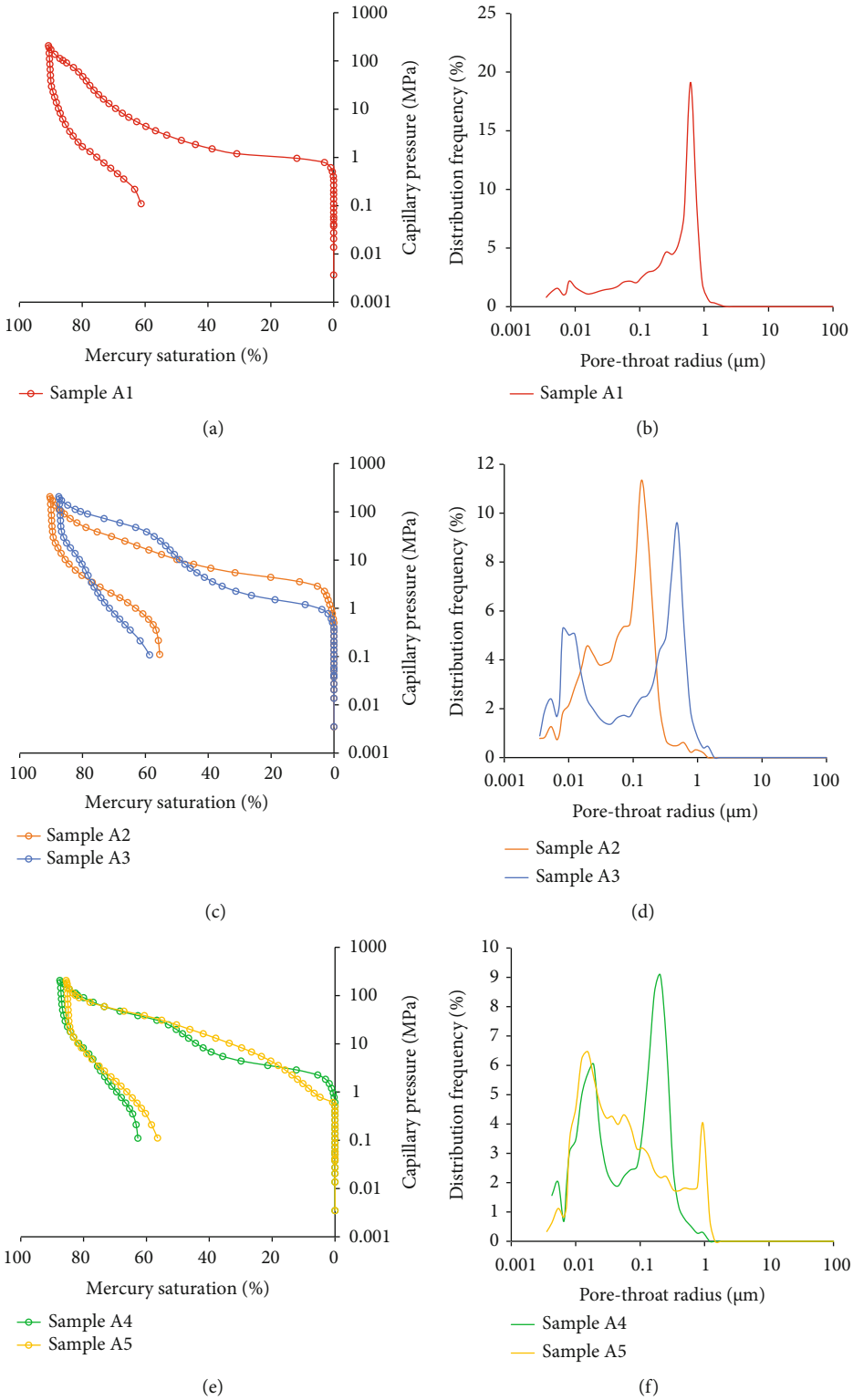

Figure 5: Typical HPMI curves. The capillary pressure curve and distribution curve of pore-throat radius of type I sample (a-b). Type II samples (c-d). Type III samples (e-f).

medium, and small pores, respectively. Among the sample of type I, medium pores were widely distributed, followed by small and large pores (Figure 6(a)). In terms of type II samples, the number of small pores was increasing (Figures 6(b) and 6(c)), which was approximate with the number of medium pores. Besides, the distribution of small pores accounted for the majority of type III (Figures 6(d) and 6(e)), while large pores were the least. The results above indicate that medium pores were widely developed in the Chang 6_3 sublayer, which was a crucial factor for the reservoir quality.

Table 2: Parameters from the HPMI experiment.

Sample ID	Category	Displacement pressure (MPa)	Median pressure (MPa)	Median radius (μm)	Sorting coefficient	Mercury saturation (%)	Efficiency of mercury withdrawal (%)
A1	I	0.40	2.46	0.29	2.22	90.78	32.51
A2	II	0.61	10.33	0.07	1.62	90.40	38.65
A3		0.51	11.78	0.06	2.50	87.58	33.03
Average		0.56	11.05	0.07	2.06	88.99	35.84
A4	III	0.79	19.01	0.03	1.96	87.54	28.32
A5		0.61	24.31	0.03	2.20	85.57	34.03
Average		0.70	21.66	0.03	2.08	86.56	31.17

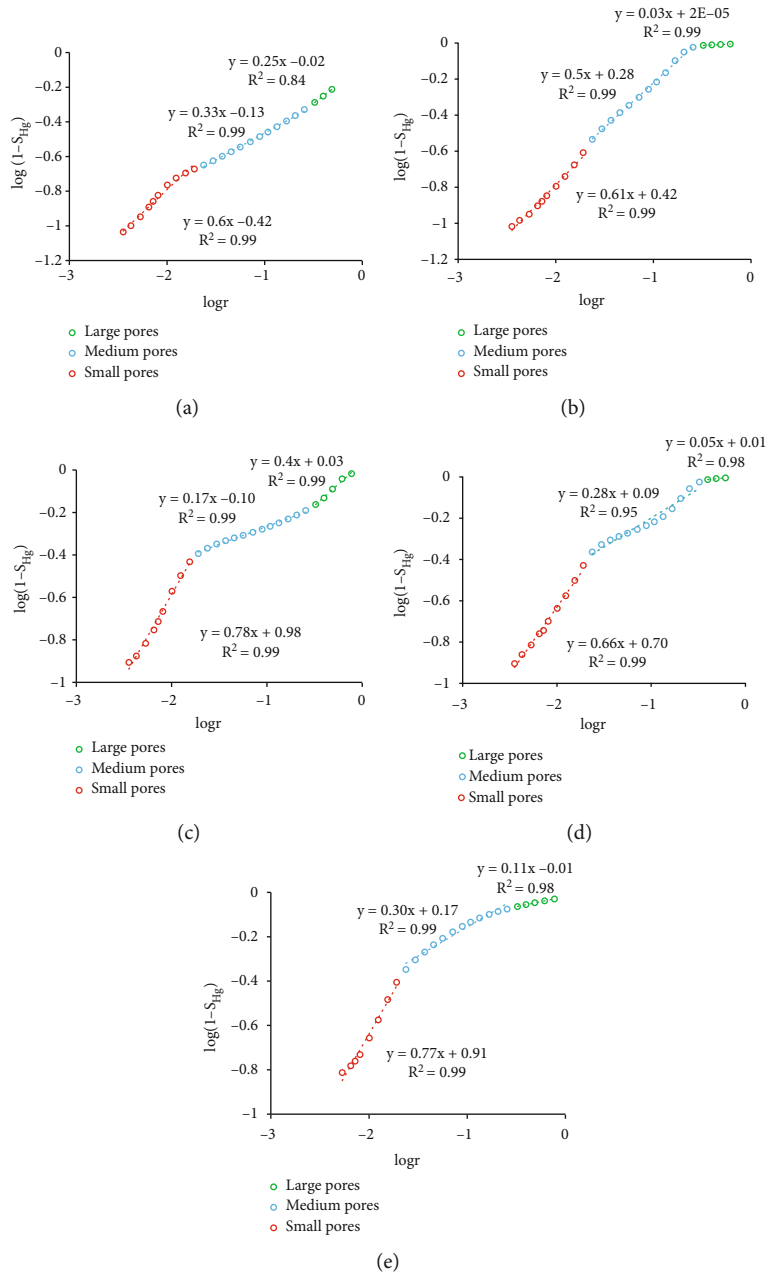

Figure 6: The relationship between the log $(1 - S_{Hg})$ and log (r) of pores corresponding to samples A1-5 (a-e), respectively.

Table 3: Fractal characteristics of the Late Triassic Chang 6_3 sublayer, Yanchang Formation.

Sample ID	Large pores				Medium pores				Small pores			
	D_{P-1}	R^2	ϕ_1 (%)	K_1 (mD)	D_{P-2}	R^2	ϕ_2 (%)	K_2 (mD)	D_{P-3}	R^2	ϕ_3 (%)	K_3 (mD)
A1	2.75	0.84	2.78	0.024	2.67	0.99	2.99	0.021	2.40	0.99	1.04	0.00001
A2	2.97	0.99	0.17	0.045	2.50	0.99	2.71	0.039	2.39	0.99	1.06	0.00234
A3	2.60	0.99	1.19	0.162	2.83	0.99	1.63	0.007	2.22	0.99	1.37	0.00003
A4	2.95	0.98	2.56	0.074	2.72	0.95	1.18	0.050	2.34	0.99	1.56	0.00026
A5	2.89	0.98	2.53	0.043	2.70	0.99	1.94	0.002	2.23	0.99	1.34	0.00009

Notes: D_{P-1}, D_{P-2}, and D_{P-3}: the fractal dimensions of large pores, medium pores, and small pores. ϕ_1, ϕ_2, and ϕ_3: the porosity of large pores, medium pores, and small pores. K_1, K_2, and K_3: the permeability of large pores, medium pores, and small pores. R^2: correlation coefficient.

The fractal dimensions (D_{P-1}, D_{P-2}, and D_{P-3}), porosity (ϕ_1, ϕ_2, and ϕ_3), and permeability contributions (K_1, K_2, and K_3) corresponding to large, medium, and small pores are calculated in Table 3 for further discussion. The D_{P-1} was the maximum with an average of 2.83, ranging from 2.60 to 2.97. The permeability of large pores is maximum with a mean value of 0.07 mD, showing that the permeability of Chang 6_3 sublayer was mainly contributed by a small number of large pores in study area. Then, the D_{P-2} ranged from 2.50 to 2.83 with an average of 2.69 while its porosity was the maximum with an average of 2.09%. It can be concluded that the medium pores mainly provided reservoir space. The D_{P-3} is 2.22 to 2.40, with a mean value of 2.31, and the permeability contribution is 0.0005 mD. Compared with large pores and medium pores, small pores made less contribution to permeability and porosity. The fractal dimensions of large pores were larger than that of the medium pores and small pores, indicating that the former had strong heterogeneity, and relatively discrete distribution. Medium pores and small pores have relatively uniform and regular pore distribution. Therefore, the fractal dimension has a positive correlation with the complexity of pore-throat structure, which is close to the previous studies [19–23].

5. Discussions

5.1. The Pore-Throat Structure Effect on the Petrophysical Characteristics. Two main inflection points, dividing the curve as large, medium, and small pores, were found according to the correlation between log $(1 - S_{Hg})$ and log (r) of each sample in Figure 7. In accordance with the coordinates of inflection points and the pore-throat radius of large pores, small pores and medium pores were obtained to be more than 0.3 μm, less than 0.02 μm and between 0.02 μm and 0.3 μm, respectively.

Together with the distribution curves of pore-throat radius, fractal curves, images of CTS (Figure 7), and the parameters of HPMI (Table 4), the pore-throat structures from typical samples were analyzed. The pore-throat structures of sample A1 were mainly large pores and medium pores, the pore types principally consisted of large residual intergranular pores and feldspar dissolved pores, with good connectivity, storage capacity, and seepage ability, but grains are poorly sorted. The pore-throat structures of sample A3 were mainly medium pores and small pores, the pore types consist of residual intergranular pores and throat with good connectivity and seepage ability, but grains are poorly sorted. The pore-throat structures of sample A4 were dominated with more small pores and followed medium pores, pore types were mainly composed of intergranular dissolution pores with small reservoir space, moderate connectivity, and good sorting.

In summary, we consider that the wide distribution of medium pores is of great significance in evaluating reservoir storage capacity and seepage capacity. The distribution of large pores was too limited to improve the quality of the reservoir. Although small pores can be observed, the storage capacity and seepage ability of the small pores are weak in the study area, therefore, the influence on the reservoir is not as strong as that of the medium pores.

5.2. The Relationship between the Fractal Dimension and Petro-Physical Characteristics. A larger fractal dimension can represent a more complex pore-throat structure and lower porosity as well as permeability of the reservoirs. The scatter plot (Figure 8) was obtained based on the fractal dimensions D_{P-1}, D_{P-2}, and D_{P-3} and porosity as well as permeability. As shown in Figure 8, the porosity and permeability were in inverse proportion to fractal dimension. The D_{P-1}, D_{P-2}, and D_{P-3} showed a negative correlation with porosity, in which D_{P-2} had the strongest correlation. Permeability had a negative correlation with D_{P-2} and no correlation with D_{P-1} and D_{P-3}. Therefore, the storage space and permeability of the reservoir were mainly contributed by medium pores. The distribution of medium pores had a great effect on the storage capacity and seepage capacity of reservoir.

5.3. The Parameters of Pore-Throat Structure Influence on the Fractal Dimension. Fractal theory can quantitatively describe the complexity and heterogeneity of pore structure [9, 10, 19–23]. The fractal dimension of the Chang 6_3 sublayer was calculated in this study, the results indicated that the larger fractal dimension, the more complex of pore-throat structure, which was consistent with previous researches [24–28].

The pore-throat structure was analyzed by plotting a scatter plot between fractal dimension and HPMI parameters (Figure 9). The fractal dimensions (D_{P-3}) of small pores showed a negative relationship with sorting coefficient

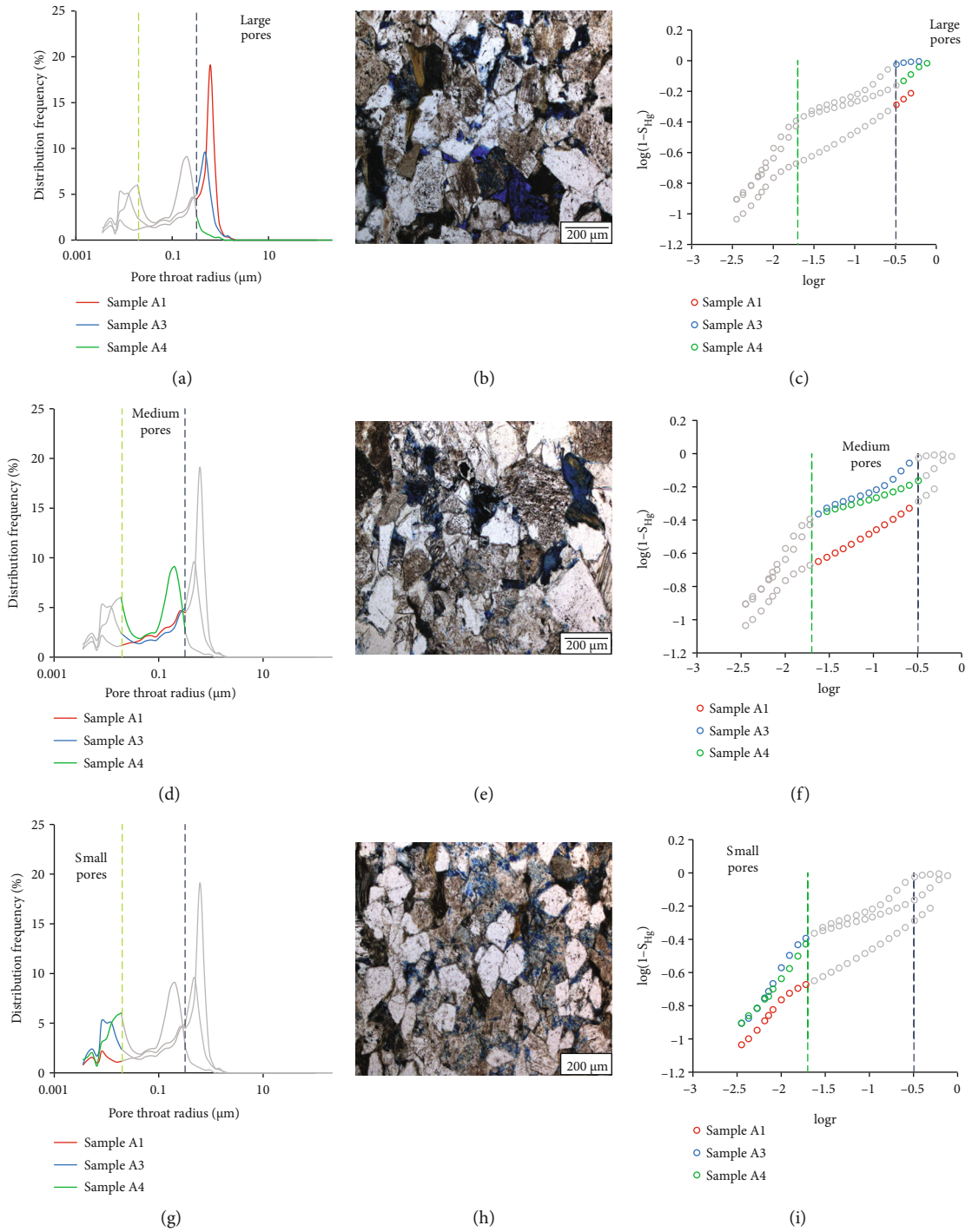

Figure 7: The pore-throat radius distribution curves of typical samples (a, d, g). The results of CTS of sample A1, A3, and A4 (b, e, h), respectively. The fractal curves of typical samples (c, f, i), and they are naturally divided into three parts by similar turning points.

Table 4: The HPMI parameters of the typical samples.

Sample ID	Displacement pressure (MPa)	Median radius (μm)	Sorting coefficient	Mercury saturation (%)	Efficiency of mercury withdrawal (%)	Porosity (%)	Permeability (mD)
A1	0.40	0.2982	2.22	90.78	32.51	10.83	0.048
A3	0.51	0.0624	2.50	87.58	33.03	8.28	0.042
A4	0.78	0.0387	1.96	87.54	28.32	6.49	0.031

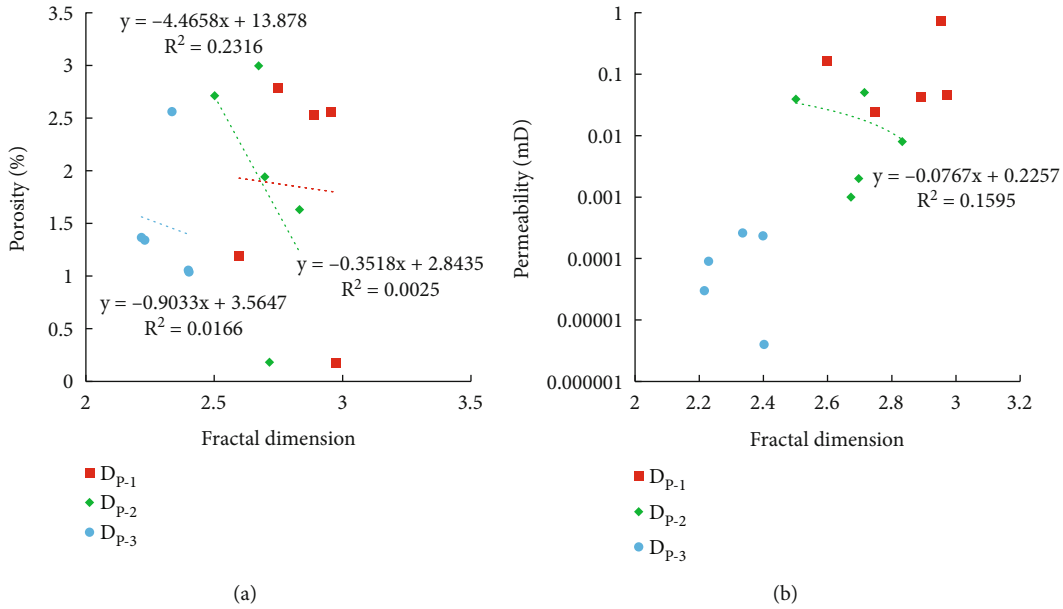

Figure 8: Fractal dimension versus porosity (a), permeability (b).

(Figure 9(b)) and capillary pressure (Figure 9(e)) and a positive relationship with efficiency of mercury withdrawal (Figure 9(d)). The results confirmed that the sorting feature and connectivity of small pores will become better as the fractal dimension increases. Moreover, the correlation between small pores and other parameters was not obvious, and the storage capacity and seepage ability of small pores were weak as discussed in Section 5.1, showing that small pores had weak effect on the pore-throat structure.

The D_{P-2} exhibited a negative correlation with median pore-throat radius (Figure 9(a)) and a positive correlation with sorting coefficient (Figure 9(b)) and variation coefficient (Figure 9(f)). The median pore-throat radius reflected the concentrated distribution of pores. With the decrease of the median pore-throat radius, the distribution of the medium pores became inhomogeneous. Meanwhile, homogeneity of medium pores was influenced by the sorting coefficient and variation coefficient. For instance, homogeneity of medium pores increases while the sorting coefficient and variation coefficient decrease. Thus, medium pores occupy a determining effect in the homogeneity of tight reservoirs.

A negative correlation between D_{P-2} with the maximum mercury saturation (Figure 9(c)) and the efficiency of mercury withdrawal (Figure 9(d)) can be observed. Under the same pressure, the maximum mercury saturation was positively correlated with reservoir storage capacity. The efficiency of mercury withdrawal and reservoir connectivity also showed a positive correlation. Both maximum mercury saturation and mercury withdrawal efficiency of medium pores will decrease with the increasing fractal dimension, which illustrated that the more complex the pore-throat structure, the weaker the storage capacity and connectivity of the pores.

In a word, the fractal dimensions (D_{P-2}) of medium pores showed a negative correlation with median radius of pore-throat, maximum mercury saturation, the mercury withdrawal efficiency, and capillary pressure and a positive correlation with sorting coefficient and variation coefficient, indicating that there is an extremely strong correlation between medium pores and pore-structure parameters. Hence, the size, complexity, and distribution of medium pores determined the reservoir storage space and connectivity of the reservoir.

5.4. The Mechanism of Mineral Composition Effect on Fractal Dimension. The complexity of pore-throat structure was affected by their mineral content and composition in the tight sandstone reservoirs [49–51]. It is shown in Figure 10, the relationship between fractal dimension and the content of rock-forming minerals (quartz and feldspar) was analyzed. It is obvious that a negative correlation between quartz and fractal dimensions (D_{P-2} and D_{P-3}) was obtained in Figure 10(a). Quartz, with strong compaction resistance and dissolution resistance, which could preserve the pore space and improve the homogeneity of pore-throat structures. Thereby, following the decrease of quartz content lead to an increase of complexity, heterogeneity, and fractal dimensions of medium and small pores. Moreover, a positive correlation between feldspar content and fractal dimensions D_{P-2} and D_{P-3} was revealed in Figure 10(b). If feldspar content increases, fractal dimensions D_{P-2} and D_{P-3} do. On account of feldspar widely existed in the study area that various pores with different types, sizes, and complex structures were formed by dissolution of feldspar in the diagenetic process. Although the pore space of the reservoir increased with feldspar content, the complex pore types decreased their fluid seepage capacity.

As discussed above, the content of quartz and feldspar has a certain influence on the complexity of medium pores

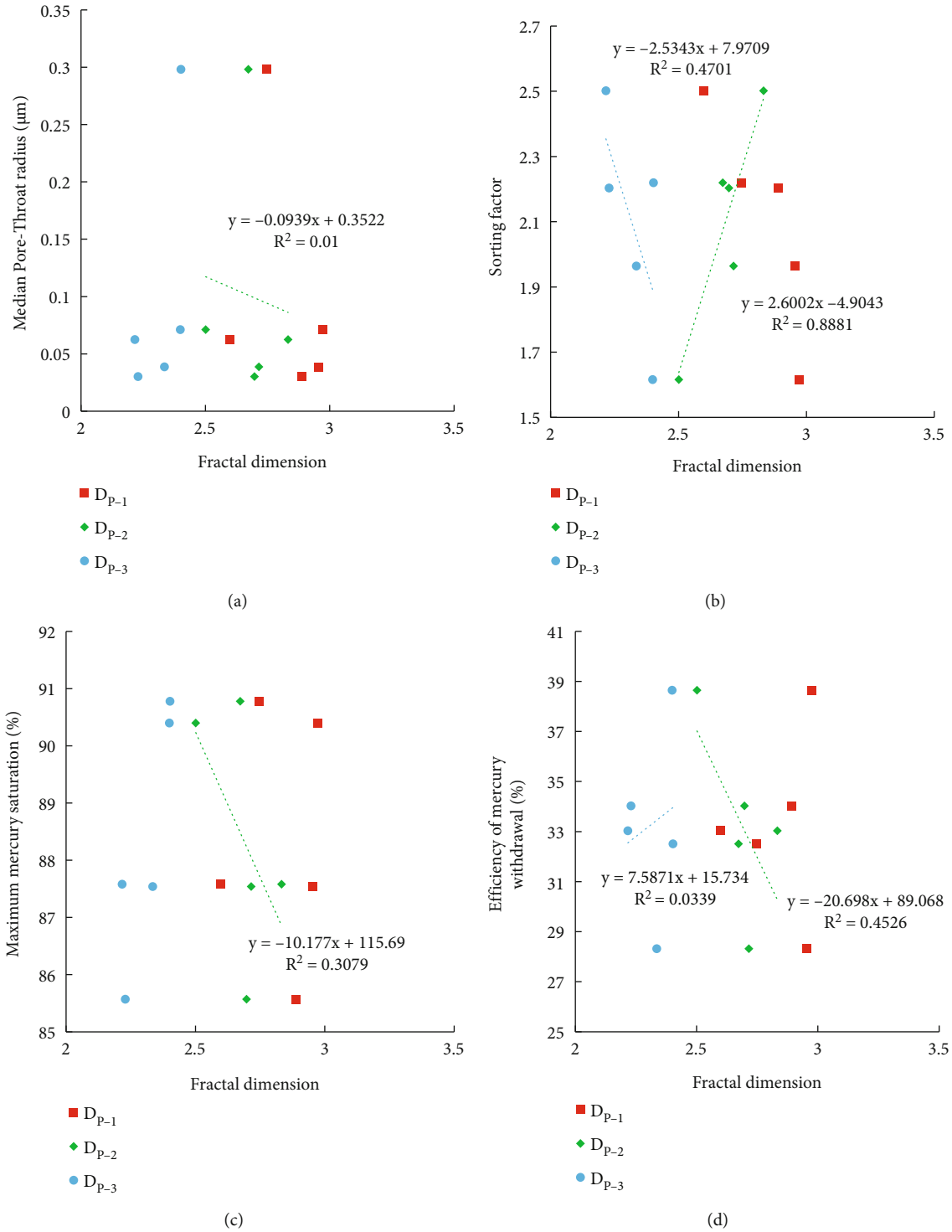

Figure 9: Continued.

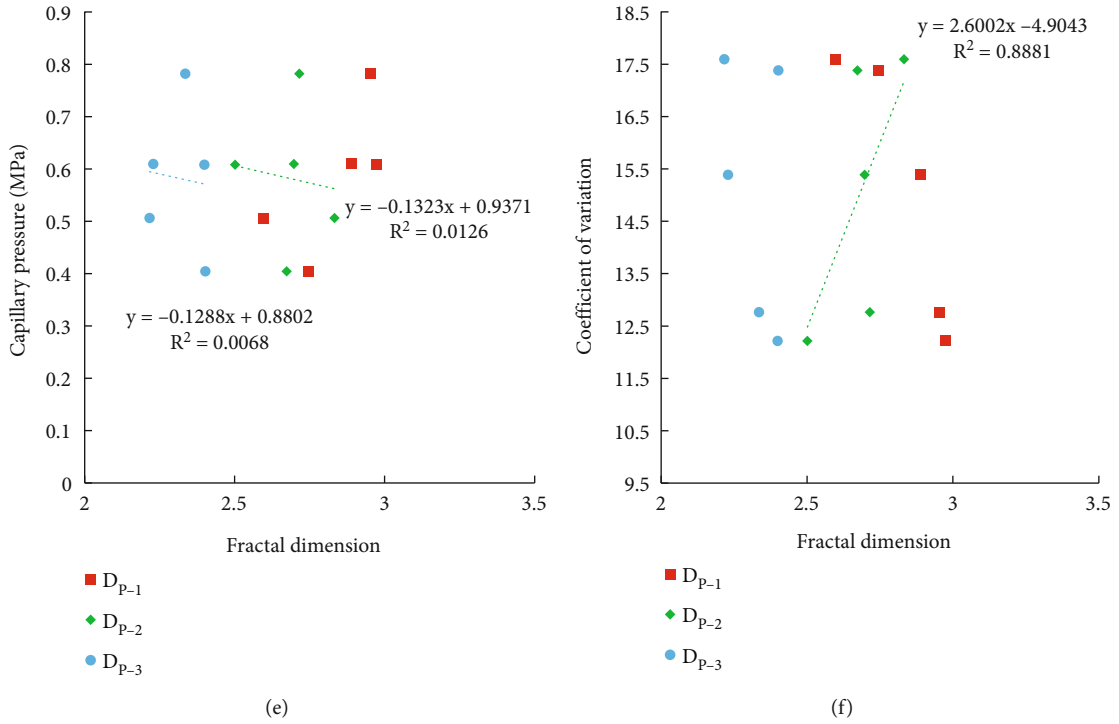

Figure 9: Fractal dimension versus median pore-throat radius (a), sorting coefficient (b), maximum mercury saturation (c), efficiency of mercury withdrawal (d), capillary pressure (e), and variation coefficient (f).

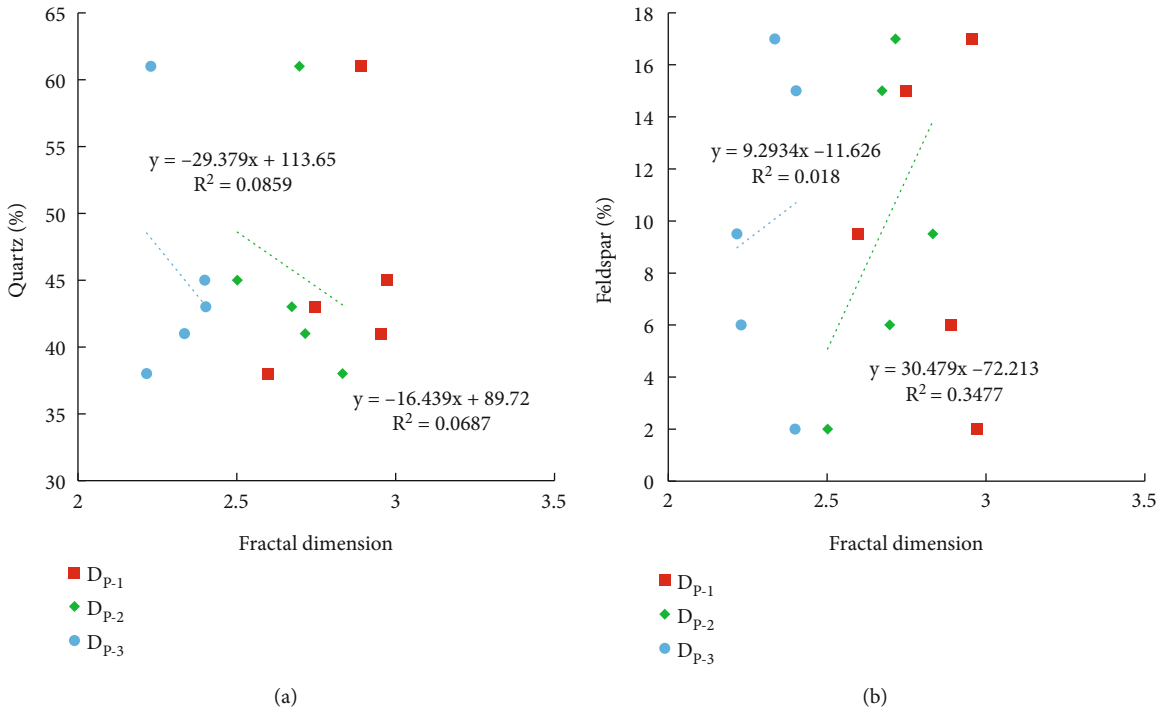

Figure 10: Fractal dimension versus quartz (a), feldspar (b).

and small pores, by which medium pores are strongly influenced with the maximum correlation coefficient. Therefore, reservoir space and seepage capacity are further affected by the complexity and heterogeneity of medium pores.

6. Conclusions

(1) The pore types of the samples mainly consist of intergranular pores, feldspar dissolved pores, and

intergranular dissolved pores. Quartz and feldspar are the main mineral composition, while clay mineral and carbonate mainly comprise these samples' interstitial materials

(2) The D_{P-1} ranged from 2.60 to 2.97 with a mean value of 2.83, the D_{P-2} from 2.50 to 2.83 with a mean value of 2.69, and the D_{P-3} from 2.22 to 2.40 with a mean value of 2.31. Therefore, large pores have the largest fractal dimension due to their complex structure and strong heterogeneity

(3) The D_{P-2} shows a negative correlation with porosity, permeability, maximum mercury saturation, and mercury withdrawal efficiency and a positive correlation with feldspar content, sorting coefficient, and variation coefficient. Thus, reservoir space and seepage capacity of samples are determined by the size, complexity, and distribution of medium pores

(4) The storage capacity of the medium pores enhances by increasing of the quartz and feldspar content in the light of both the compaction resistance for quartz and the dissolutive for feldspar. However, the types, sizes, and structures of medium pores also became complex with the increase of feldspar content, resulting in the reduction of fluid seepage capacity

Data Availability

The underlying data is not available.

Additional Points

Highlights. (i) The pore-throat structure for the Chang 6_3 sublayer was analyzed by comprehensive methods. (ii) The fractal characteristics of the pore-throat structure were quantitatively defined into large, medium, and small pores. (iii) The relationship between fractal dimension and micropore-throat structure was discussed. (iv) The influencing mechanism of mineral composition on fractal dimension was discussed.

Conflicts of Interest

The authors declare that they have no known competing financial interests or personal relationships that could have appeared to influence the work reported in this paper.

Authors' Contributions

Zhuo Han was responsible for sampling, data analysis, and he wrote the manuscript. Fanrong Wei was responsible for the resources. Qian Zhang was responsible for the investigation. Pingtian Fan and Jiantao Gong were also responsible for the resources. Erping Ma was also responsible for data analysis. Chao Deng, Xin Cheng, and Hanning Wu modified the manuscript. Yanan Zhou designed the research plan and wrote and modified the manuscript.

Acknowledgments

Financial support for this study was jointly provided by the National Natural Science Foundation of China (Grant Nos. 91855211, 42074075) and Liu Baojun Geoscience Youth Science Foundation (DMSM20190042). We would like to thank Dongmeng Zhang, Teng Li, and Longyun Xing, who assisted in the sample collections. The Nanniwan Oil Production Plant of Yanchang Oilfield Company was thanked for providing the drill cores used in this study.

References

[1] S. A. Holditch, "Tight gas sands," *Journal of Petroleum Technology*, vol. 58, no. 6, pp. 86–93, 2006.

[2] C. N. Zou, G. S. Zhang, and Z. Yang, "Concepts, characteristics, potential and technology of unconventional hydrocarbons: on unconventional petroleum geology," *Petroleum Exploration and Development*, vol. 40, no. 4, pp. 413–428, 2013.

[3] C. Z. Jia, C. N. Zou, and J. Z. Li, "Assessment criteria, main types, basic features and resource prospects of the tight oil in China," *Acta Petrolei Sinica*, vol. 33, no. 3, p. 343, 2012.

[4] C. N. Zou, S. Z. Tao, and Z. Yang, "New advance in unconventional petroleum exploration and research in China," *Bulletin of Mineralogy, Petrology and Geochemistry*, vol. 31, no. 4, p. 312, 2012.

[5] H. Yang, S. X. Li, and X. Y. Liu, "Characteristics and resource prospects of tight oil and shale oil in Ordos Basin," *Acta Petrolei Sinica*, vol. 34, no. 1, 2013.

[6] J. Z. Zhao, D. X. Wang, and L. Y. Sun, "Origin of the Ordovician gas and its accumulation patterns in Northwestern Ordos Basin," *Oil & Gas Geology*, vol. 36, no. 5, 2015.

[7] Z. C. Cheng, W. G. Liu, S. H. Li et al., "High-efficiency separation of CO_2 from CO_2-CH_4 gas mixtures via gas hydrates under static conditions," *Separation and Purification Technology*, vol. 296, 2022.

[8] H. Y. Deng, G. L. Sheng, H. Zhao et al., "Integrated optimization of fracture parameters for subdivision cutting fractured horizontal wells in shale oil reservoirs," *Journal of Petroleum Science and Engineering*, vol. 212, article 110205, 2022.

[9] D. Z. Ren, H. P. Zhang, Z. Z. Wang, B. Y. Ge, D. K. Liu, and R. J. Zhang, "Experimental study on microscale simulation of oil accumulation in sandstone reservoir," *Frontiers in Physics*, vol. 10, no. 10, 2022.

[10] D. K. Liu, T. Tian, C. Y. Zhao, L. Sun, and D. Z. Ren, "The role of mineralogical stratifications in controlling brine flow behavior in shale at a pore-scale perspective based on integrated imaging and compositional methods," *Journal of Petroleum Science and Engineering*, vol. 214, article 110409, 2022.

[11] H. Gao and H. Z. Li, "Pore structure characterization, permeability evaluation and enhanced gas recovery techniques of tight gas sandstones," *Journal of Natural Gas Science and Engineering*, vol. 28, pp. 536–547, 2016.

[12] M. M. Meng, H. K. Ge, W. M. Ji, Y. H. Shen, and S. Su, "Monitor the process of shale spontaneous imbibition in co-current and counter- current displacing gas by using low field nuclear magnetic resonance method," *Journal of Natural Gas Science and Engineering*, vol. 27, pp. 336–345, 2015.

[13] D. K. Liu, D. Z. Ren, K. Du, Y. R. Qi, and F. Ye, "Impacts of mineral composition and pore structure on spontaneous

imbibition in tight sandstone," *Journal of Petroleum Science and Engineering*, vol. 201, article 108397, 2021.

[14] M. Brai, C. Casieri, F. De Luca, P. Fantazzini, M. Gombia, and C. Terenzi, "Validity of NMR pore-size analysis of cultural heritage ancient building materials containing magnetic impurities," *Solid State Nuclear Magnetic Resonance*, vol. 32, no. 4, pp. 129–135, 2007.

[15] C. R. Clarkson, M. Freeman, L. He et al., "Characterization of tight gas reservoir pore structure using USANS/SANS and gas adsorption analysis," *Fuel*, vol. 95, pp. 371–385, 2012.

[16] H. A. Nooruddin, M. Enamul Hossain, H. Al-Yousef, and T. Okasha, "Comparison of permeability models using mercury injection capillary pressure data on carbonate rock samples," *Journal of Petroleum Science and Engineering*, vol. 121, pp. 9–22, 2014.

[17] H. L. Liu, H. C. Wang, and H. Zhang, "Nano pore network of asphalt in Xiaoheba Formation in the eastern Sichuan Basin and its significance for reservoir formation," *Natural Gas Geoscience*, vol. 31, no. 6, p. 818, 2020.

[18] H. X. Huang, R. X. Li, F. Y. Xiong et al., "A method to probe the pore-throat structure of tight reservoirs based on low- field NMR: insights from a cylindrical pore model," *Marine and Petroleum Geology*, vol. 117, article 104344, 2020.

[19] Y. Q. Qu, W. Sun, R. D. Tao, B. Luo, L. Chen, and D. Ren, "Pore-throat structure and fractal characteristics of tight sandstones in Yanchang Formation, Ordos Basin," *Marine and Petroleum Geology*, vol. 120, article 104573, 2020.

[20] D. K. Liu, Z. L. Gu, R. X. Liang et al., "Impacts of pore-throat system on fractal characterization of tight sandstones," *Geofluids*, vol. 2020, Article ID 4941501, 17 pages, 2020.

[21] R. D. Zhong, R. X. Li, D. K. Liu, Y. H. Li, N. Liu, and F. Yang, "Quantifying fractal dimension in integrated experimental data of tight sandstones," *Geofluids*, vol. 2019, Article ID 6463473, 19 pages, 2019.

[22] P. Li, M. Zheng, H. Bi, S. T. Wu, and X. R. Wang, "Pore throat structure and fractal characteristics of tight oil sandstone: a case study in the Ordos Basin, China," *Journal of Petroleum Science and Engineering*, vol. 149, pp. 665–674, 2017.

[23] X. Y. Zhong, Y. S. Zhu, T. Jiao et al., "Microscopic pore throat structures and water flooding in heterogeneous low- permeability sandstone reservoirs: A case study of the Jurassic Yan'an Formation in the Huanjiang area, Ordos Basin, Northern China," *Journal of Asian Earth Sciences*, vol. 219, article 104903, 2021.

[24] J. G. Liu, L. S. Qu, Z. Y. Song et al., "Fracability evaluation method and influencing factors of the tight sandstone reservoir," *Geofluids*, vol. 2021, Article ID 7092143, 15 pages, 2021.

[25] Q. Feng, S. Xu, X. Xing, W. Zhang, and S. Wang, "Advances and challenges in shale oil development: a critical review," *Advances in Geo-Energy Research*, vol. 4, no. 4, pp. 406–418, 2020.

[26] D. Hao, C. Yang, and D. X. Liu, "Pore throat structure and NMR fractal characteristics of tight sandstone reservoirs in Baibao Oilfield, Ordos Basin," *Journal of Xi'an Shiyou University*, vol. 36, no. 5, 2021.

[27] S. Dong, L. Zeng, C. Xu et al., "A novel method for extracting information on pores from cast thin-section images," *Computers & Geosciences*, vol. 130, pp. 69–83, 2019.

[28] D. J. Feng and K. H. Xiao, "Constant velocity mercury injection and nuclear magnetic resonance in evaluation of tight sandstone reservoirs in western Sichuan Basin," *Petroleum Geology & Experiment*, vol. 43, no. 2, p. 368, 2021.

[29] H. B. Zeng, F. R. Wang, J. Luo, T. Tao, and S. Q. Wu, "Characteristics of pore structure of inter salt shale oil reservoir by low temperature nitrogen adsorption and high pressure mercury pressure methods in Qianjiang Sag," *Bulletin of Geological Science and Technology*, vol. 40, no. 5, pp. 242–252, 2021.

[30] Z. D. Lu, C. L. Liu, and Q. B. Zang, "Application of high-pressure mercury injection parameters in nuclear magnetic resonance: a case study of Heshui Area, Ordos Basin," *Bulletin of Geological Science and Technology*, vol. 1, no. 1, 2021.

[31] C. Shen, C. X. Ouyang, D. Ruan, and Q. Wu, "Fractal characteristics of pore structure of tight sandstone reservoirs: a case study of Fuyang oil layer in Xinli oilfield," *China Sciencepaper*, vol. 14, no. 12, 2019.

[32] J. Lai and G. Wang, "Fractal analysis of tight gas sandstones using high-pressure mercury intrusion techniques," *Journal of Natural Gas Science and Engineering*, vol. 24, pp. 185–196, 2015.

[33] K. Li, "Analytical derivation of Brooks-Corey type capillary pressure models using fractal geometry and evaluation of rock heterogeneity," *Journal of Natural Gas Science and Engineering*, vol. 73, 2010.

[34] H. Yang, J. Fu, H. He, Z. Zhang, and X. Deng, "Formation and distribution of large low-permeability lithologic oil regions in Huaqing, Ordos Basin," *Petroleum Exploration and Development*, vol. 39, no. 6, pp. 683–691, 2012.

[35] J. L. Yao, X. Q. Deng, and Y. D. Zhao, "Characteristics of tight oil in Triassic Yanchang Formation, Ordos Basin," *Petroleum Exploration and Development*, vol. 40, no. 2, pp. 161–169, 2013.

[36] P. Li, C. Jia, Q. Liu, M. Zheng, and Z. Huang, "The characteristics of movable fluid in the Triassic lacustrine tight oil reservoir: a case study of the Chang 7 member of Xin'anbian Block, Ordos Basin, China," *Marine and Petroleum Geology*, vol. 102, pp. 126–137, 2019.

[37] H. Yang, J. H. Fu, and X. S. Wei, "Natural gas formation characteristics in Ordos Basin," *Chinese journal of Periodical of Gas*, vol. 25, no. 4, 2005.

[38] W. H. Li, X. Liu, Q. Zhang et al., "Deposition evolution of Middle-Late Triassic Yanchang Formation in Ordos Basin," *Journal of Northwest University*, vol. 49, no. 4, 2019.

[39] J. H. Fu, X. Q. Deng, X. L. Zhang, A. X. Luo, and J. X. Nan, "Relationship between deep water sandstone and tight oil of the Triassic Yanchang Formation in Ordos Basin," *Journal of Palaeogeography*, vol. 15, no. 5, 2013.

[40] Q. L. Wei, C. H. Wang, and J. F. Liu, "Characteristics and main controlling factors of Chang 63 reservoir in Fanjiachuan area, Ordos Basin," *Lithologic Reservoirs*, vol. 34, no. 2, 2022.

[41] J. Lai, G. W. Wang, S. Wang et al., "Review of diagenetic facies in tight sandstones: diagenesis, diagenetic minerals, and prediction via well logs," *Earth-Science Reviews*, vol. 185, pp. 234–258, 2018.

[42] Z. Y. Zhang and A. Weller, "Fractal dimension of pore-space geometry of an Eocene sandstone formation," *Geophysics*, vol. 79, no. 6, pp. D377–D387, 2014.

[43] B. B. Mandelbrot, "On the geometry of homogeneous turbulence, with stress on the fractal dimension of the iso-surfaces of scalars," *Journal of Fluid Mechanics*, vol. 72, no. 3, p. 401, 1975.

[44] S. Kulesza and M. Bramowicz, "A comparative study of correlation methods for determination of fractal parameters in

surface characterization," *Applied Surface Science*, vol. 239, pp. 196–201, 2014.

[45] Y. He and N. S. Wu, "A new method for determining fractal dimension of pore structure," *Experimental Petroleum Geology*, vol. 21, no. 4, p. 372, 1999.

[46] D. D. Hong, J. Cao, T. Wu, S. S. Dang, W. X. Hu, and S. P. Yao, "Authigenic clay minerals and calcite dissolution influence reservoir quality in tight sandstones: insights from the central Junggar Basin, NW China," *Energy Geoscience*, vol. 1, no. 1-2, pp. 8–19, 2020.

[47] R. L. Folk, *Petrology of Sedimentary Rocks*, Hemphill Publishing, 1974.

[48] X. H. Guo, C. Q. Tan, and J. H. Zhao, "Different influence of diagenesis on micro pore-throat characteristics of tight sandstone reservoirs: case study of the Triassic Chang 7 member in Jiyuan and Zhenbei areas, Ordos Basin," *Natural Gas Geoscience*, vol. 32, no. 6, p. 826, 2021.

[49] X. B. Ge, J. J. Li, and S. F. Lu, "Fractal characteristics of tight sandstone reservoir using mercury intrusion capillary pressure: a case of tight sandstone reservoir in Jizhong depression," *Lithologic Reservoirs*, vol. 29, no. 5, p. 106, 2017.

[50] Y. Q. Qu, W. Sun, H. N. Wu et al., "Impacts of pore-throat spaces on movable fluid: implications for understanding the tight oil exploitation process," *Marine and Petroleum Geology*, vol. 137, article 105509, 2022.

[51] H. X. Huang, R. X. Li, W. T. Chen et al., "Revisiting movable fluid space in tight fine-grained reservoirs: a case study from Shahejie shale in the Bohai Bay Basin, NE China," *Journal of Petroleum Science and Engineering*, vol. 207, article 109170, 2021.